Cumhuriyet Science Journal
CSJ

e-ISSN: 2587-246X
ISSN: 2587-2680

Cumhuriyet Sci. J., Vol.39-4 (2018) 1036-1051

Structural, Spectroscopic and Anti-cancer Properties of Hydroxy- and Sulfonamide-Azobenzene Platinum (II) Complexes: DFT and Molecular Docking Studies

Sultan ERKAN

Cumhuriyet University, Yıldızeli Vocational School, Chemical and Chemical Company Technology, Sivas, TURKEY

Received: 04.05.2018; Accepted: 02.11.2018 *http://dx.doi.org/10.17776/csj.421027*

Abstract. The three platinum (II) complexes ([Pt(L1)(DMSO)Cl], [Pt(L2)(DMSO)Cl] and [Pt(L2)$_2$]) bearing the bidentate ligands sulphonamide-((E)-2-(4-methylphenylsulfonamido)-2′,6′-difluoroazobenzene, HL1) and hydroxy-azo-2,6-difluorobenzene ((E)-2-((2,6-difluorophenyl)diazenyl)phenol, HL2) were optimized with the optimum levels of B3LYP/6-31+G(d) and B3LYP/LANL2DZ/6-31+G(d) level. The structural parameters (bond lengths and ligand angles), IR and ^{1}H, ^{13}C and ^{19}F-NMR spectra obtained from the optimized structures were compared with the experimental data and the results were found to be consistent with the experimental results. Experimental inhibition activities against A2780 and A2780CP70 cancer cells were compared with quantum chemical parameters such as HOMO energy (E_{HOMO}), LUMO energy (E_{LUMO}), LUMO-HOMO energy vacancy (ΔE), hardness (η), softness (σ), electronegativity (χ) and chemical potential (μ). The relationship between the molecular structure with the biological activity was examined and E_{LUMO} order was found to be compatible with the experimental inhibition efficiency ranking. Molecular electrostatic potential (MEP) maps were studied of ligands and complexes exhibiting anti-cancer properties and for ligands and complexes, regions of attachment to cancer cells were determined. In addition, electrostatic potential (ESP) charges obtained from MEP maps of ligands and complexes were ranked according to their ease of binding to the cancer cell. The obtained ranking was found to be in accordance with the experimental inhibition efficiency order. For studied ligands and complexes, molecular docking studies were carried out with the Hex.8.0.0 program. The target proteins (PDB ID: 4M5W and 5FI4, respectively) corresponding to the A2780 and A2780CP70 cell lines were selected in the literature. The interaction energies of 4M5W and 5FI4 target proteins with HL1 and HL2 ligands were calculated to be -300.02, -240.80 and -336.64, -247.04 kJ/mol, respectively. The binding energies between the complexes and 4M5W and 5FI4 target proteins were calculated to be -387.52, -285.44, -364.88 and -399.63, -297.8, -385.323 kJ/mol. According to these results, the experimental and calculated inhibition efficiency order was found to be compatible.

Keywords**:** Platinum (II) complexes, DFT and Molecular Docking Studies.

Hidroksi- ve Sülfonamid- Azobenzen Platin (II) Komplekslerinin Yapısal, Spektroskopik ve Anti-Kanser Özellikleri: DFT ve Moleküler Yerleştirme Çalışmaları

Özet. Bidentat ligandlar olan sülfonamid-((E)-2-(4-metilfenilsülfonamido)-2',6'-diizoazobenzen, HL1) ve hidroksi-azo-2,6-diflorobenzen ((E)-2-((2,6-diflorofenil)diazenil)fenol, HL2) taşıyan üç platin (II) kompleksi ([Pt(L1)(DMSO)Cl], [Pt(L2)(DMSO)Cl] ve [Pt(L2)$_2$]) en uygun seviye olarak belirlenen B3LYP/6-31+G(d) ve B3LYP/LANL2DZ/6-31+G(d) seviyesi ile optimize edildi. Optimize yapılardan elde edilen yapısal parametreler (bağ uzunluklar ve bağ açıları), IR ve ^{1}H, ^{13}C ve ^{19}F-NMR kimyasal kaymaları deneysel veriler ile

* Corresponding author. *Email address:* *sultanerkan58@gmail.com*

kıyaslandı ve sonuçlar deneysel sonuçlar ile uyumlu olduğu görüldü. A2780 ve A2780CP70 kanser hüclerine karşı deneysel inhibisyon etkinlikleri HOMO enerjisi (E_{HOMO}), LUMO enerjisi (E_{LUMO}), LUMO-HOMO enerji boşluğu (ΔE), sertlik (η), yumuşaklık (σ), elektronegativite (χ) ve kimyasal potansiyel (μ) gibi kuantum kimyasal parametreler ile kıyaslandı. Aktivite yapı arasındaki ilişki incelendi ve E_{LUMO} deneysel inhibisyon etkinlik sıralaması ile bire bir uyumlu bulundu. Anti-kanser özellik gösteren ligand ve komplekslerin moleküler elektrostatik potansiyel (MEP) haritaları incelendi ve HL1 ve HL2 ligandları ve Comp. (1)-(3) için kanser hücrelerine bağlanma bölgeleri belirlendi. Ayrıca MEP haritalarından elde edilen elektrostatik potansiyel (ESP) yükleri ile ligandlar ve komplekslerin kanser hücresine bağlanma kolaylıklarına göre sıralamaları yapıldı. Elde edilen sıralama deneysel inhibisyon etkinlik sıralaması uyumlu bulundu. Çalışılan ligand ve kompleksler için Hex.8.0.0 programı ile moleküler yerleştirme çalışmaları yapıldı. A2780 ve A2780CP70 hücre çizgisine karşılık gelen hedef proteinler (PDB ID:4M5W ve 5FI4, sırasıyla) literatürde seçildi. 4M5W ve 5FI4 hedef proteinleri ile HL1 ve HL2 ligandaların etkileşim enerjileri sırasıyla -300.02, -240.80 ve -336.64, -247.04 kJ/mol olarak hesaplandı. Kompleksler ile 4M5W ve 5FI4 hedef proteinleri arasındaki bağlanma enerjileri -387.52, -285.44, -364.88 ve -399.63, -297.8, -385.323 kJ/mol olarak hesaplandı. Bu sonuçlara göre deneysel ve hesaplanan inhibisyon etkinlik sıralaması uyumlu bulundu.

***Anahtar Kelimeler*:** Platinum (II) kompleksleri, DFT ve Moleküler Yerleştirme Çalışmaları.

1. INTRODUCTION

Azobenzene has been extensively used in many fields such as molecular biology, pharmacology and chemistry [1-10]. The azobenzene and derivatives such as 2-(arylazo) pyridines, 2-(arylazo) pyrimidines and 2-(arylazo) imidazoles are very interesting compounds in coordination chemistry due to their strong M-L bonds resulting from interesting redox behaviors and strongπ-acceptor character [11]. Cisplatin and carboplatin are FDA-approved chemotherapeutic drugs used as part of first line therapy for several different types of cancer [12,13]. Platinum (II) complexes are relatively important in the treatment of cancer. For anti-cancer platinum-based drugs, mainly experimental studies have quite extensive and there are major economic losses in these studies [14-20].

In this study, we aimed to investigate of experimentally synthesized HL1 [21] and HL2 ligands and cisplatin complexes [22] containing these ligands in terms of structural, spectroscopic and anti-cancer properties by computational chemistry methods. Therefore, in this study, the optimum level is determined as B3LYP/LANL2DZ/6-31+G(d) level for complexes. Based on this level, ligands are studied at B3LYP/6-31+G(d) level. In this work, the experimentally synthesized HL1, HL2 and [Pt(L1)(DMSO)Cl] (Comp. (1)), [Pt(L2)(DMSO)Cl] (Comp. (2)) and [$Pt(L2)_2$] (Comp. (3)) compounds are studied. Structural and spectroscopic (IR and NMR) analyzes of the mentioned compounds are performed at the best level. IC50 values have been reported for the compounds mentioned by Samper et al. some quantum chemical parameters were associated with structure and biological activity. The molecular electrostatic potential (MEP) maps and electrostatic potential (ESP) charge derived from these maps of HL1, HL2 and their platinum (II) complexes are examined in detail. In addition, molecular docking studies are conducted against the cancer cell line being studied.

2. CALCULATION METHOD

The input files of the studied compounds were made using GaussView 6.0 [23]. All calculations were performed with Gaussian 09 AML64L-Revision-C.01 [24]. Optimized molecular structures were carried out with Chemcraft. exe 1.8.0.178 licensed program [25]. HF [26] and DFT/B3LYP [27] method which are quite common methods are preferred for ligands and complexes. CEP-31G [28] and LANL2DZ/6-31+G(d) basis sets are selected for the complexes. 6-31+G(d) basis set are used in calculated of ligands.

3. RESULT AND DISCUSSION

3.1 Benchmark analysis

For the Comp. (1)-(3), the correlation coefficient (R^2) values derived from distribution graphs according to these parameters and experimental and calculated bond lengths and bond angles are given in Table 1. The first level chosen in the calculations is the HF/CEP-31G level used for trans-platin (II) oxime complexes by Sayın and Karakaş [29-31]. The second calculation level is B3LYP/LANL2DZ/6-31+G(d), which is quite common in the computational studies of transition metal complexes. The structural parameters obtained from the structures optimized by two calculation methods for Comp. (1)-(3) are given in Table 1.

Table 1. The experimental and calculated with HF and B3LYP methods and CEP-3G and LANL2DZ basis sets structure parameters and their correlation coefficients.

Comp. (1)				Comp.(2)				Comp.(3)			
Bond length (Å)	**Exp.**	**Cal.1***	**Cal.2***	**Bond length (Å)**	**Exp.**	**Cal.1***	**Cal.2***	**Bond length (Å)**	**Exp.**	**Cal.1***	**Cal.2***
Pt-Cl1	2.2967	2.3962	2.4318	Pt-O1	1.9930	1.9889	2.0054	Pt-O2	1.9866	2.0201	2.0396
Pt-S2	2.2368	2.4763	2.4439	Pt-N2	2.0050	2.0706	2.0305	Pt-N4	1.991	2.0851	2.0341
Pt-N1	2.0180	2.0938	2.0479	Pt-S1	2.2248	2.4757	2.4374	Pt-O1	1.9916	2.0201	2.0396
Pt-N3	2.0370	2.0190	2.0017	Pt-Cl1	2.3105	2.4112	2.4499	Pt-N2	1.9997	2.0850	2.0341
R^2	-	**0.8655**	**0.9448**	**R^2**	-	**0.8841**	**0.9601**	**R^2**	-	**0.4352**	**0.4323**
Bond angles (°)											
N1-Pt-N3	84.99	82.50	83.33	O1-Pt-N2	90.31	88.66	90.83	O2-Pt-N4	90.32	86.94	89.02
N1-Pt-S2	94.46	98.03	97.88	O1-Pt-S1	170.58	172.25	169.58	O2-Pt-O1	80.64	86.82	83.42
N3-Pt-S2	174.31	178.58	178.30	N2-Pt-S1	99.04	99.10	99.38	N4-Pt-O1	170.7	172.02	170.25
N1-Pt-Cl1	175.27	170.51	172.63	O1-Pt-Cl1	83.25	88.28	85.75	O2-Pt-N2	170.38	172.02	170.25
N3-Pt-Cl1	90.29	95.06	93.89	N2-Pt-Cl1	173.15	176.93	176.02	N4-Pt-N2	99.16	99.68	99.11
S2-Pt-Cl1	90.27	84.60	84.76	S1-Pt-Cl1	87.46	83.97	84.10	O1-Pt-N2	89.94	86.94	89.02
R^2	-	**0.9882**	**0.9920**	**R^2**	-	**0.9955**	**0.9973**	**R^2**	-	**0.9933**	**0.9989**

*Cal.1 = HF/CEP-31G and Cal.2 = B3LYP/LANL2DZ/6-31+G (d)

When the R^2 values were investigated in Table 1 for the Comp. (1)-(3), the closest level to 1 was determined as B3LYP/LANL2DZ/6-31+G(d) level. This level was preferred for other calculations of this study.

3.2 Optimize structures

Optimized structures obtained in the gas phase with B3LYP/6-31G+(d) for the ligands and B3LYP/LANL2DZ/6-31G+(d) for the complexes are given in Figures 1 and 2, respectively. Optimized structures of ligands and complexes was done using Chemcraft.exe 1.8.0.178 program.

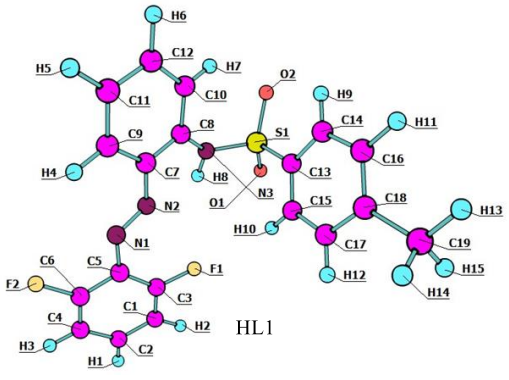

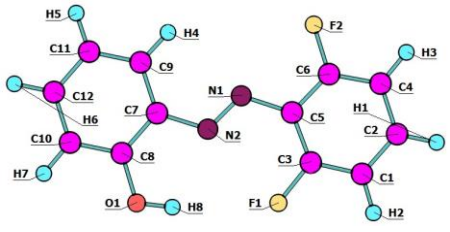

HL2

Figure 1. The obtained optimized structures for the HL1 and HL2 using B3LYP/6-31+G(d) level.

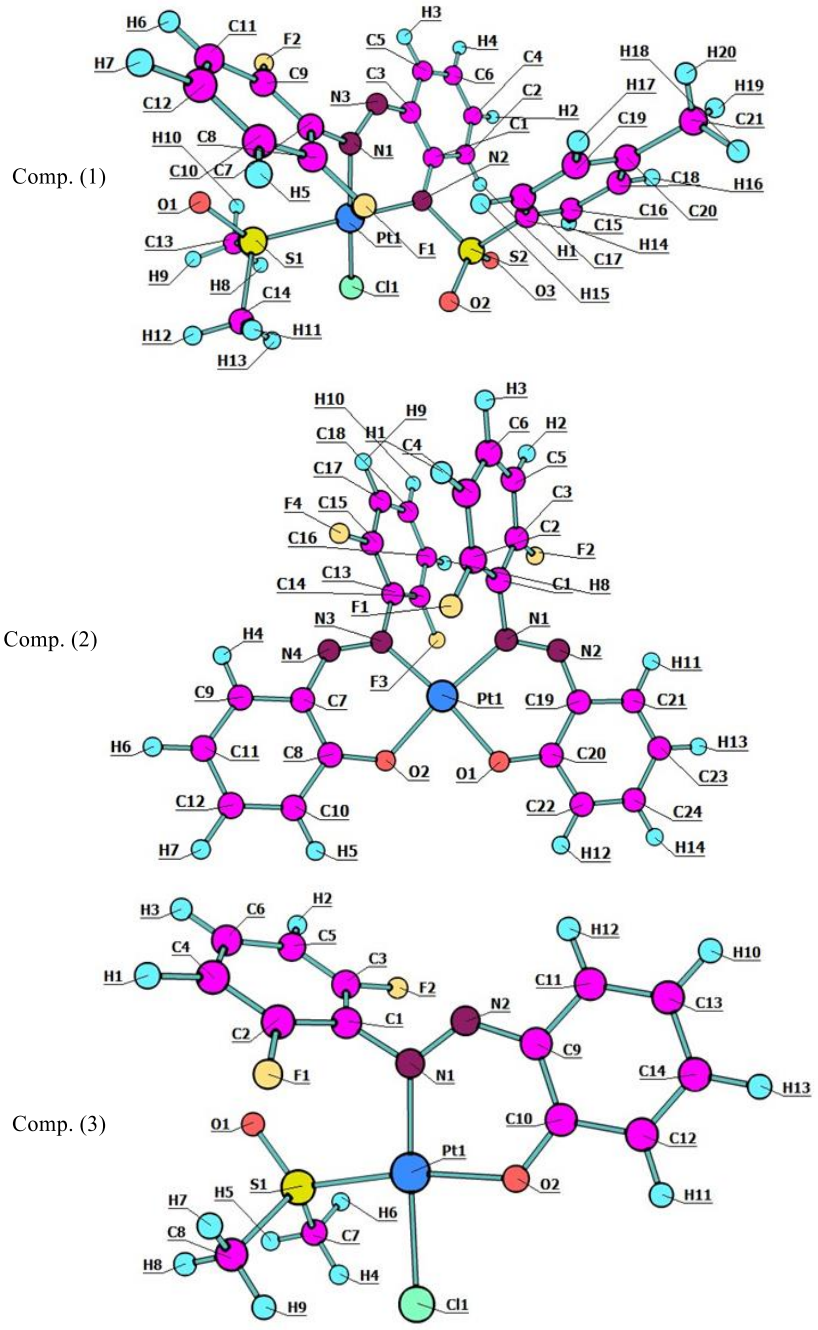

Figure 2. Optimized structures for the Comp. (1)-(3) at B3LYP/LANL2DZ/6-31+G(d) level.

3.3 IR analysis

Harmonic frequencies obtained from the out files of the B3LYP/6-31+G(d) and B3LYP/LANL2DZ/6-31+G (d) for the ligand and complexes, were compared to the experimental frequencies with the aid of an animation program [32-34]. According to this comparison, the bond stretching modes were labeled. From the calculated frequencies, the bond stretching frequencies with the highest the molar absorption coefficient ($M^{-1}cm^{-1}$) were taken into account. The experimental and calculated bond stretching for the HL1, HL2 and Comp. (1)-(3) are given in Table 2 as comparative.

Table 2. Experimental and calculated vibrational frequencies (cm^{-1}) of the mentioned ligands calculated at B3LYP/6-31+G(d) level and their assignment.

HL1			HL2		
Exp.*	**Cal.**	**Assign.**	**Exp.****	**Cal.**	**Assign.**
3299	3492.81	ν_{N-H}	3099	3589.56	ν_{O-H}
1613	1658.76	$\nu_{Caro-Caro\ (difluorophenyl)}$	3066	3232.30	$\nu_{Caro-H\ (difluorophenyl)}$
1594	1625.10	$\nu_{Caro-Caro}$	2922	3219.04	ν_{Caro-H}
1477	1548.84	$\nu_{N=N}$	2852	3205.68	ν_{Caro-H}
1390	1476.55	ν_{Caro-N}	1614	1658.16	$\nu_{Caro-Caro}+\nu_{N=N}$
1338	1433.60	$\nu_{S=O}$	1589	1631.67	$\nu_{Caro-Caro}$
1165	1272.82	$\nu_{Caro-N}+\nu_{Caro-F}$	1470	1545.94	$\nu_{N=N}$
1092	1132.92	ν_{Caro-S}	1411	1520.55	ν_{Caro-O}
1028	1082.79	$\nu_{Caro-S}+\nu_{Caro-N}$	1358	1506.10	$\nu_{Caro-N}+\nu_{Caro-F}$
926	1045.97	ν_{Caro-F}	1323	1393.64	$\nu_{Caro-Caro}+\nu_{N=N}$
759	842.80	$\nu_{Caro-N}+\nu_{Caro-S}$	1289	1304.07	$\nu_{Caro-F}+\nu_{Caro-O}$
			1271	1295.87	$\nu_{Caro-O}+\nu_{Caro-N}+\nu_{Caro-F}$
			1227	1279.74	$\nu_{Caro-O}+\nu_{Caro-N}+\nu_{Caro-F}$
			1146	1226.08	ν_{Caro-N}
			1111	1176.82	$\nu_{Caro-N}+\nu_{Caro-O}$
			1025	1042.89	ν_{Caro-F}
			818	912.76	$\nu_{Caro-N}+\nu_{Caro-F}$
			785	871.12	$\nu_{Caro-Caro}+\nu_{Caro-O}+\nu_{Caro-N}$
			754	820.10	$\nu_{Caro-Caro}$

*Experimental values were taken from reference [21]. **Experimental values were taken from reference [22].

Table 3. Experimental and calculated vibrational frequencies (cm^{-1}) of Comp. (1)-(3) calculated at B3LYP/LANL2DZ/6-31+G(d) level and their assignment.

Comp. (1)			Comp. (2)			Comp. (3)		
Exp.	**Cal.**	**Assign.**	**Exp.**	**Cal.**	**Assign.**	**Exp.**	**Cal.**	**Assign.**
3014	3242.82	νCaro-H	3060	3246.91	νCaro-H	3064	3243.11	νCaro-H
2927	3106.26	νCH_3(Caro)	3007	3227.15	νCH_3(DMSO)	2923	3226.76	νCaro-H(dfp*)
2853	3096.57	νCH3(DMSO)	2920	3206.04	νCaro-H	2852	3201.8	νCaro-H
1616	1660.89	νCaro-Caro	2851	3094.97	νCH_3(DMSO)	1734	1670.51	νCaro-Caro
1596	1646.45	νCaro-Caro	1610	1669.64	νCaro-Caro+νN=N+νC-O	1605	1669.93	νCaro-Caro+νCaro-Caro(dfp*)
1468	1514.27	νN=N	1599	1648.72	νCaro-Caro	1593	1644.06	νCaro-Caro(dfb*)
1423	1504.25	νCaro-Caro	1477	1513.5	νN=N+νC-O+νCaro-N	1526	1574.8	νN=N
1317	1450.86	νN=N	1394	1459.84	νN=N+νCaro-N	1471	1516.7	νCaro-O
1279	1343.17	νN=N+νCaro-Caro	1307	1416.04	νC-O+νCaro-N	1380	1449.37	νCaro-N
1249	1308.9	νCaro-F+νN=N	1291	1337.24	νN=N+νC-O+νCaro-N	1308	1332.83	νC-O+νCaro-N
1141	1205.45	νCaro-N	1250	1303.62	νC-F+νN=N+νC-O+νCaro-N	1238	1305.5	νC-O+νCaro-Caro
1084	1088.39	νCaro-S	1146	1202.46	νCaro-N	1180	1263.1	νCaro-N+νN=N
1018	1075.93	$\nu S\text{-}CH_3$	1009	1056.02	$\nu S\text{-}CH_3$	1140	1201.56	νN=N+νCaro-N
948	1019.27	νCaro-F	959	1016.85	νCaro-F	1015	1025.56	νCaro-F
914	967.56	νPt-N	786	970.72	νPt-N	944	966.03	νPt-N
856	957.35	νS-O	753	818.02	$\nu O\text{-}S(CH_3)$	847	902.38	νPt-N
764	816.12	$\nu O\text{-}S(CH_3)$				779	821.83	νPt-O
						747	793.46	wCaro-H

Dfp*: difluorophenly, w: wagging taken from reference [32]

In Table 2, the calculated harmonic frequencies corresponding to the experimental vibrational frequencies of the HL1 and HL2 ligands and their respective labeling are given. When the results are examined; The experimental and calculated frequencies for HL1 and HL2 ligands seem to be compatible with one another. Computational chemistry methods are very useful in supporting

many experimental studies on the assignment of vibration frequencies. The experimental frequency at 3299 cm^{-1} was calculated to be 3492.81 cm^{-1} and it was observed that these frequency of vibration corresponded to N-H bond stretching. The experimental frequency of 1613 cm-1 was calculated as 1658.76 cm^{-1} and corresponded to Caro-Caro bond stretching in diflurophenyl. The experimental frequency at 1594 $cm^{-1}$was calculated as 1625.10 cm^{-1} and corresponded to the stretching of aromatic carbons. The experimental frequency determined as 1477 cm^{-1} is calculated as N=N bond stretching of 1548.81 cm^{-1}. The frequency calculated as 1433.60 cm^{-1} corresponds to the S=O bond stretching. This calculated frequency is experimentally labeled to frequency within 1338 cm^{-1}. The experimental frequency at 1165 cm^{-1} was calculated to be 1272.82 cm^{-1}. At this frequency value, Caro-N and Caro-F bond stretching were observed. The experimental frequency at 1092 cm^{-1} was calculated as 1082.79 cm^{-1} and labeled as Caro-S and Caro-N bond stretching. The experimental frequency of 926 cm^{-1} was calculated as 1045.97 cm^{-1} and labeled as Caro-F bond stretching. The experimental frequency of 759 cm^{-1} was calculated as 842.80 cm^{-1} and Caro-N and Caro-S bond stretching was observed. Similar comments can be made for the ligand HL2 and Comp. (1)-(3) in Table 3.

3.4 NMR spectra

Nuclear Magnetic Resonance (NMR) spectroscopy is one of the most important analytical technique used to determine the structures of the molecular and supramolecular. When combined with molecular modeling and quantum chemistry methods, the feasibility of NMR spectroscopy is useful quite to solve various structural problems. Theoretical calculations of NMR parameters are useful for restructuring molecular and supramolecular structures from experimental NMR data [35].

^{1}H, ^{13}C and ^{19}F-NMR chemical shifts calculated phase with the GIAO method for the HL1, HL2 ligands at B3LYP/6-31G(d)+ level and Comp. (1)-(3) at B3LYP/LANL2DZ/6-31G+(d) level in the gas were given in Table 4 and Table 5, respectively.

Table 4. The experimental and the calculated at the GIAO method B3LYP/6-31G(d)+ level of the ^{1}H and ^{13}C-NMR chemical shift values for HL1 and HL2 ligands and this chemical shift corresponding atom assignment.

HL1			HL1			HL2			HL2		
^{1}H-NMR			^{13}C-NMR			^{1}H-NMR			^{13}C-NMR		
Assign.	Calc.	Exp.	Assign.	Calc.	Exp.	Assign.	Calc.	Exp.	Assign.	Calc.	Exp.
19H	8.13	9.71	8C	160.80	153.1	16H	7.78	12.3	8C	159.92	156.2
25H	8.01	7.89	3C	151.49	144.7	18H	7.39	7.99	11C	154.95	152.5
35H	7.74	7.76	11C	139.69	142.9	4H 19H	7.19 7.01	7.44-7.32	3C	151.43	138.8
16H 33H 18H	7.64 7.45 7.37	7.69-7.66	36C 29C	138.94 138.67	137.6	9H 5H 17H	6.91 6.80 6.76	7.12-7.03	10C	136.59	134.5
38H	7.23		10C	136.57	136.7				15C	131.59	133.6
4H	7.21	7.60-7.58	15C	130.23	133.3				7C	127.85	130.9
37H	6.92		7C	127.98	132.5				2C	125.72	128.9
9H	6.90	7.53	2C	126.28	130.3				14C	114.90	120.2
5H	6.85	7.25	30C	123.55 123.25	130.1				13C	112.41	118.61
17H	6.83	7.16	32C	122.85 122.70	127.9				12C 1C	109.85 109.06	112.1
42H	2.43	2.22	14C	117.34	125.9				6C	108.59	
41H	2.35	2.22	13C	115.01	123.9						
40H	1.74	2.22	12C	109.65	123.5						
			1C 6C	108.71 107.71	119.8						
			39C	22.88	21.3						

Table 5. The experimental and the calculated at the GIAO method B3LYP/ LANL2DZ/6-31G+(d) level of the ^{1}H and ^{13}C-NMR chemical shift values for Comp. (1)-(3) ligands and this chemical shift corresponding atom assignment.

Comp. (1)		Comp. (1)		Comp. (2)		Comp. (2)		Comp. (3)		Comp. (3)	
^{1}H-NMR		^{13}C-NMR		^{1}H-NMR		^{13}C-NMR		^{1}H-NMR		^{13}C-NMR	
10H	8.12	6C	336.52	10H	8.12	6C	336.52	9H	4.81	3C	378.34
13H	5.23	7C	112.40	13H	5.23	7C	112.41	10H	4.61	4C	150.06
14H	5.30	8C	268.55	14H	5.29	8C	268.55	11H	5.39	5C	114.21
15H	6.11	9C	128.63	15H	6.11	9C	128.63	24H	5.17	6C	116.39
23H	6.02	11C	111.87	23H	6.02	11C	111.88	26H	2.87	7C	121.71
24H	2.26	12C	151.78	24H	2.27	12C	352.93	27H	6.40	8C	115.05
25H	3.94	17C	352.93	25H	3.94	17C	202.25	28H	6.07	19C	243.89
30H	0.37	18C	202.25	30H	0.37	18C	121.29	35H	4.81	20C	168.41
31H	5.66	19C	121.29	31H	5.67	19C	124.38	36H	4.61	21C	124.21
32H	-6.74	20C	124.38	32H	-6.74	20C	105.33	37H	5.39	22C	129.98
34H	-15.94	21C	105.33	34H	-15.94	21C	107.27	43H	5.17	23C	139.69
35H	3.98	22C	107.27	35H	3.98	22C	63.72	45H	2.87	25C	125.82
36H	13.19	29C	63.72	36H	13.19	29C	-14.02	46H	6.40	29C	378.32
44H	7.70	33C	-14.02	44H	12.55	33C	116.34	47H	6.07	30C	150.13
46H	12.55	40C	138.26	46H	7.50	40C	127.21			31C	114.22
48H	7.50	41C	122.02	48H	8.56	41C	122.46			32C	116.39
49H	8.56	42C	116.34	49H	2.75	42C	139.98			33C	121.71
51H	2.75	43C	127.20	51H	2.15	43C	19.05			34C	115.06
52H	2.15	45C	122.46	52H	2.62	45C	336.52			38C	243.85
53H	2.62	47C	139.98	53H	8.12	47C	112.41			39C	168.35
		50C	19.05			50C	268.55			40C	124.22
										41C	129.97
										42C	139.68
										44C	125.81

In Table 4, the calculated ^{1}H and ^{13}C-NMR chemical shift values for HL1 and HL2 were given and atom labeling was performed according to the experimental chemical shift values. The experimental and calculated values for the ligands according to Table 4 were in accordance with one another. The ^{1}H-NMR chemical shift value at the experimental value of 9.71 ppm was calculated to be 8.13 ppm and labeled as hydrogen number 19. The chemical shift value, which was experimentally 7.89 ppm, was calculated as 8.01 ppm and labeled as 25H. The experimental chemical shift at 7.74 ppm was calculated to be 7.76 ppm and labeled as 35H. The other experimental and calculated values with similar approaches were presented in the table and atomic assignmentwas done.

In Table 5, the calculated^{1}H and ^{13}C-NMR chemical shifts values at the GIAO method B3LYP/LANL2DZ/6-31G+(d), experimental ^{1}H and ^{13}C-NMR chemical shifts values and corresponding atom labeling ofthese values and were presented for the inorganic complexes. There were some differences between the calculated and experimental ^{1}H and ^{13}C-NMR chemical shifts. Even negative chemical shifts were obtained. While there is a harmony between the calculated NMR values and the experimental NMR values of the organic molecules, there may be a difference between the experimental and calculated chemical shift values of the complexes. The tetramethylsilane (TMS) which we use as a reference substance is a material chosen to be the most shielding effect for carbon and hydrogen atoms. For this reason, tetramethylsilane (TMS) is used when the chemical shift values of organic molecules are calculated is a preferred way to achieve closer results to the experiment. However, more shielding effect in inorganic molecules than TMS may cause them to have negative chemical shift values. Additional, the experimental ^{19}F-NMR chemical shifts values for HL2 and Comp. (1)-(3) were -120.41, -119.8 and -120.5, -121.8 and -117.36 ppm, respectively. According to the results obtained with the GIAO method B3LYP/LANL2DZ/6-31G+(d), ^{19}F-NMR chemical shift for HL2 was calculated to be -129.7 for 20F and -125.8 ppm for 21F and the calculated results were consistent with the experimental values. The experimental ^{19}F-NMR chemical shifts

for Comp. (1) are -119.8 and -120.5 ppm while the calculated ^{19}F-NMR chemical shifts are -132.8 and -139.5 ppm. The ^{19}F-NMR chemical shifts for Comp. (2) were calculated to be -35.18 and -67.45 ppm. Comp. (3) were calculated as -161.18 and -47.24 ppm.

3.5 Quantum chemical parameters

Quantum chemical parameters provide useful information for predicting chemical activity depending on the electronic structure of the molecules. The chemical activities of the molecules depend on these identifiers. Drug design can be performed by considering the interactions between molecules in chemistry. The activity of a drug candidate is estimated from its molecular identifiers. Molecular structure identifiers are parameters such as HOMO energy (E_{HOMO}), LUMO energy (E_{LUMO}), LUMO-HOMO energy gap (ΔE), hardness (η), softness (σ), electronegativity (χ) and chemical potential (μ). Some electronic identifiers of the mentioned ligands and complexes investigated in this study were calculated and the values of the calculated identifiers were given in Table 6.

Table 6. Some electronic structure identifiers of the mentioned ligands and complexes.

Parameters	HL1	HL2	Comp. (1)	Comp. (2)	Comp. (3)
E_{HOMO} (eV)	-6.4004	-6.3213	-5.8064	-6.0723	-5.3571
E_{LUMO} (eV)	-2.9715	-2.8749	-3.0115	-2.8428	-2.7035
LUMO-HOMO energy gap (ΔE)	3.4289	3.4463	2.7949	3.2295	2.6537
Hardness (η)	1.7145	1.7232	1.3975	1.6147	1.3268
Softness (σ)	0.5833	0.5803	0.7156	0.6193	0.7537
Electronegativity (χ)	4.6860	4.5981	4.4090	4.4575	4.0303
Chemical potential (μ)	-4.6860	-4.5981	-4.4090	-4.4575	-4.0303
IC50 (Against A2780)	7±2	51±4	1.0±0.3	3.4±0.7	6.5±0.1
IC50 (Against A2780CP70)	7.5±0.1	66±3	2.7±0.6	10±3	7.0±0.1
IC50 values against A2780 and A2780-CP70 were taken as reference [22].					

The correlation between the values of these descriptors and the experimentally measured IC50 values was investigated. The IC50 value is termed the half maximal inhibitor concentration and is a measure of the activity of a substance in a biochemical process. As the interaction between complexes and biological structure increases, the IC50 value decreases. The decrease in IC50 values indicates that the biological activity is high. The way in which the descriptors given in Table 6 are how they relate to the biological activity are explained below.

3.5.1 HOMO and LUMO

The molecular orbital energy diagram of the molecule is given in the Gaussian output file. HOMO and LUMO orbitals are easily seen from this energy diagram. The molecular orbital energy diagrams of the investigated the ligands and the complexes were given in Figure 3.

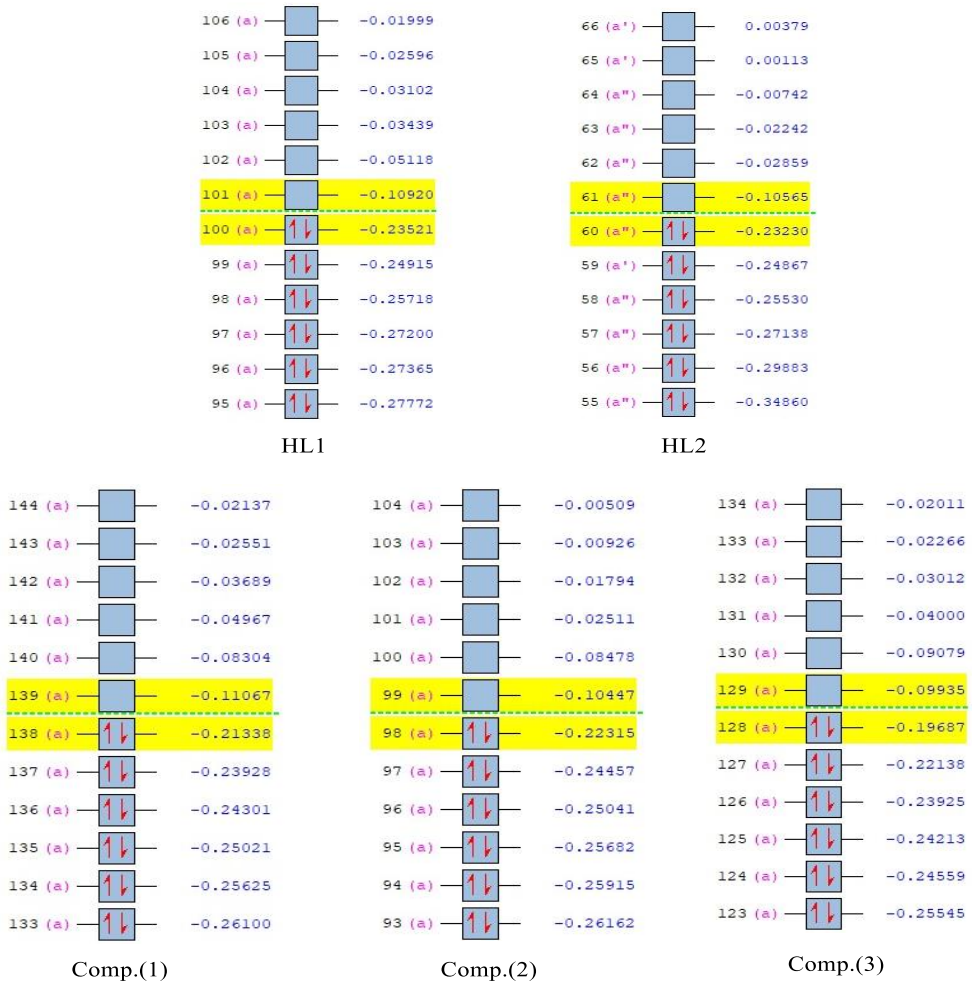

Figure 3. Molecular orbital energy diagrams from HOMO-5 to LUMO+5 of the investigated ligands andcomplexes.

If HOMO is highly energy, such a molecule tends to give electrons, whereas if LUMO has low energies, such a molecule has a high tendency to attract electrons. The IC50 values against A2780 and A2780-CP70 cancer cells and HOMO, LUMO energies of the studied ligands and complexes are given in Table 6. As seen in Table 6, the biological activities of the complexes are higher than those of the ligands according to the quantum chemical parameters. These results are in agreement with experimental results. The order of activation of the molecules studied according to HOMO and LUMO energies is given below.

Comp. (3) > Comp. (1) > Comp. (2)
HL1> HL2
} According to HOMO

Comp. (1) > Comp. (2) > Comp. (3)
HL1> HL2
} According to LUMO

3.5.2 Energy gap (ΔE)

The energy gap of a molecule depends on the LUMO and HOMO energies of the molecule.

$$\Delta E = E_{LUMO} - E_{HOMO}$$

The energy gap of a molecule indicates greater stability and low chemical reactivity. The energy gaps of the Comp. (1)-(3) and HL1, HL2 are given in Table 6. The energy gap sequence of the complexes and ligands is as follows.

Comp. (3) > Comp. (1) > Comp. (2)
HL1> HL2
} According to ΔE

3.5.3 Hardness (η), Softness (σ), Electronegativity (χ) and Chemical Potential (μ)

The first quantitative correlations for the absolute hardness, softness, absolute electronegativity and chemical potential of the molecules were proposed by R. G. Pearson in 1987 [36]. According to Pearson, absolute hardness (η) depends on softness (σ), absolute electronegativity (χ) and chemical potential (μ) depend on ionization energy (I) and electron affinity (A) and are calculated by the following equations.

$$\eta = \frac{I - A}{2}$$

$$\sigma = \frac{1}{\eta}$$

$$\chi = \frac{I + A}{2}$$

$$\mu = -\chi$$

According to the Koopmans theorem, the ionization energies and the electron affinity of the chemical species are equal to the energies of the frontier orbitals of the molecules [37].

$$I = -E_{HOMO}$$
$$A = -E_{LUMO}$$

According to these equations, when the HOMO and LUMO energies are known, the absolute hardness, softness, absolute electronegativity and chemical potential of the chemical species can be calculated. The order of the values of η, σ, χ and μwere presented in Table 6 as follows.

Comp. (3) > Comp. (1) > Comp. (2) } According to η,σ,χ and μ
HL1> HL2

When the IC50 values of experimentally synthesized ligands and complexes against A2780 and A2780-CP70 are examined, the ligands exhibit a similar tendency towards both cancer cells but have no similar tendency for complexes. For this reason, all quantum chemical parameters for the ligands were in agreement with the experimentally inhibition activity. For complexes, only LUMO energies gave results consistent with experimental inhibition activities.

3.6 Molecular electrostatic potential (MEP) maps and Electrostatic Potential (ESP)

Molecular electrostatic potential (MEP) maps are a widespread area of research foreseeing electrostatic regions in molecules. MEP maps define the region with high electron density in red color and the region with low electron density in blue color. This is also important in determining electrostatic attack and nucleophilic attack sites, respectively. MEP maps are also useful for identifying the active site of a chemical system. The MEP maps obtained with computational chemistry methods can be found in useful information in drug design. It is very important to determine the regions of interaction between the synthesized drugs and the target proteins. In addition, the electrostatic potential (ESP) charges obtained from MEP maps provide numerical data foreseeing the ease of interaction of the synthesized drug with the target protein [38-40]. The MEP maps calculated at B3LYP/LANL2DZ/6-31G+(d) levelfor complexes and at B3LYP/6-31G(d)+ level for ligands are shown in Figure 5.

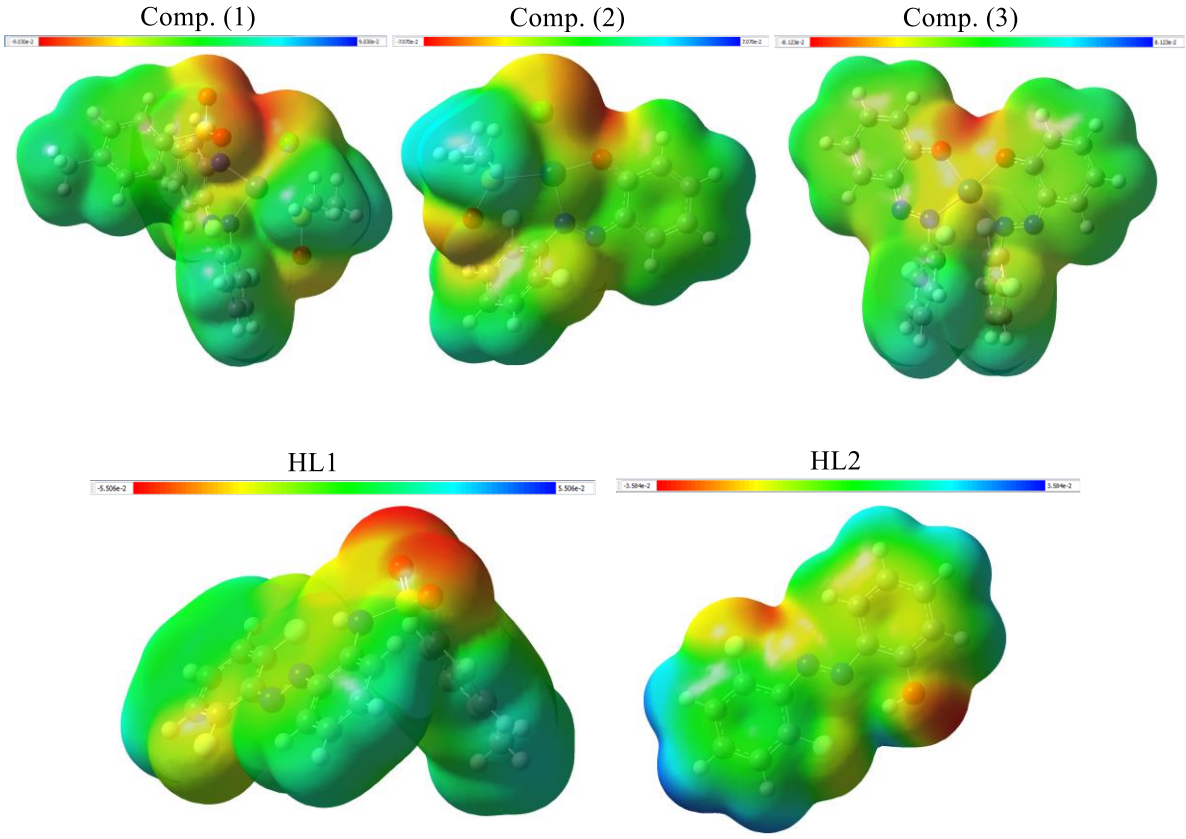

Figure 5. MEP maps and ESP charge of mentioned molecules.

When MEP maps are examined, active sites in the ligands and complexes are usually regions where oxygen atoms are present. It can be considered as electrophilic sites in regions where fluorine atoms are present. The biological activity ranking according to the IC50 values against A2870CP70 cell line given in Table 6 is as follows:

Comp. (1) > Comp. (3) > Comp. (2)

HL1 > HL2

The ESP charges densities obtained from the MEP maps for Comp. (1)-(3)are $\pm 9.030\times10^{-2}$, $\pm 7.070\times10^{-2}$ and $\pm 8.123\times10^{-2}$, respectively. ESP charges densities for HL1 and HL2 are $\pm 5.506\text{x}10^{-2}$ and $\pm 3.584\text{x}10^{-2}$. ESP charge densities derived from MEP maps are a measure of the ease of binding of the studied molecules to cancer cells. The order of binding to cancer cells according to these charge densities exhibits a similar tendency to the order of the experimentally obtained IC50 values.

3.7 Molecular Docking

In recent years, molecular docking studies have attracted considerable attention in calculation chemistry. The binding energy obtained by molecular docking among the computational chemistry methods can be correlated with the experimentally determined half-maximal inhibitor concentration (IC50) [41]. The target protein corresponding to the experimentally selected cancer cell is determined from the protein data bank and this target protein is interacted with the studied molecules by the docking program. PDB ID for A2780 and A2870CP70 cancer cells of the are determined as 4M5W and 5FI4 in the literature, respectively [42,43]. Forms of active binding with target proteins for HL1, HL2 and Comp. (1)-(3) were given in Figures 6 and 7 and the binding energies between target proteins with ligand and complexes were shown in Table 7.

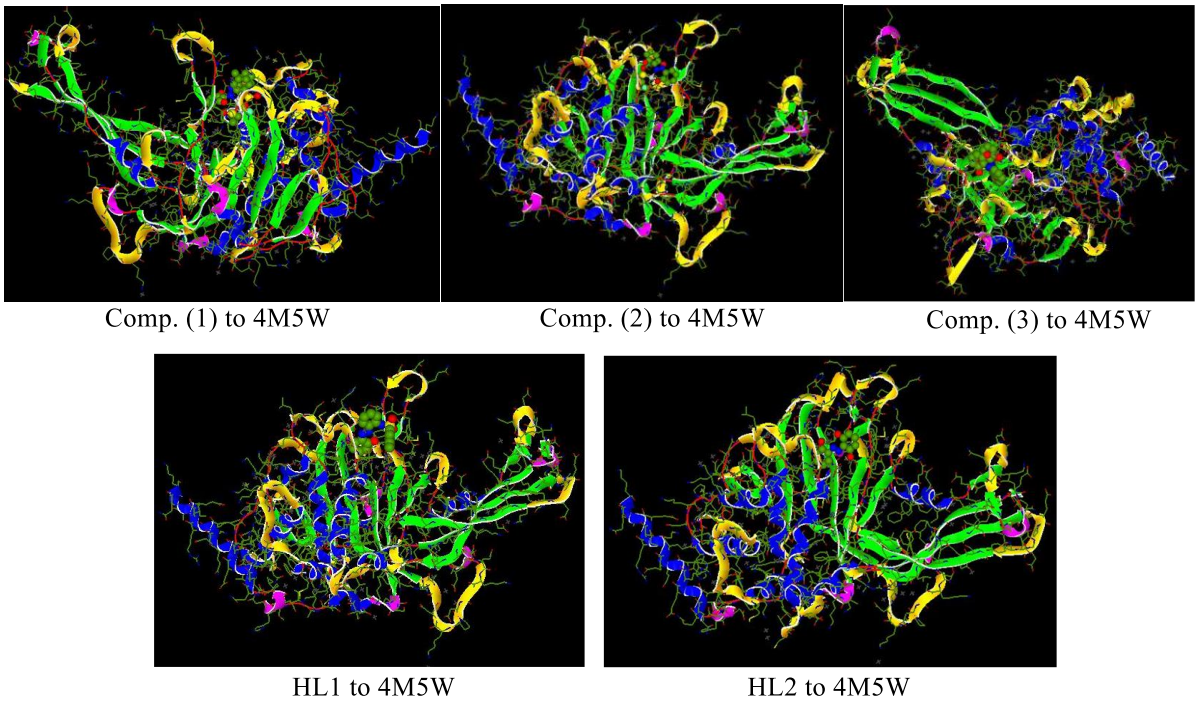

Figure 6. The binding region of the Comp. (1)-(3) and HL1, HL2 with the 4M5W target protein.

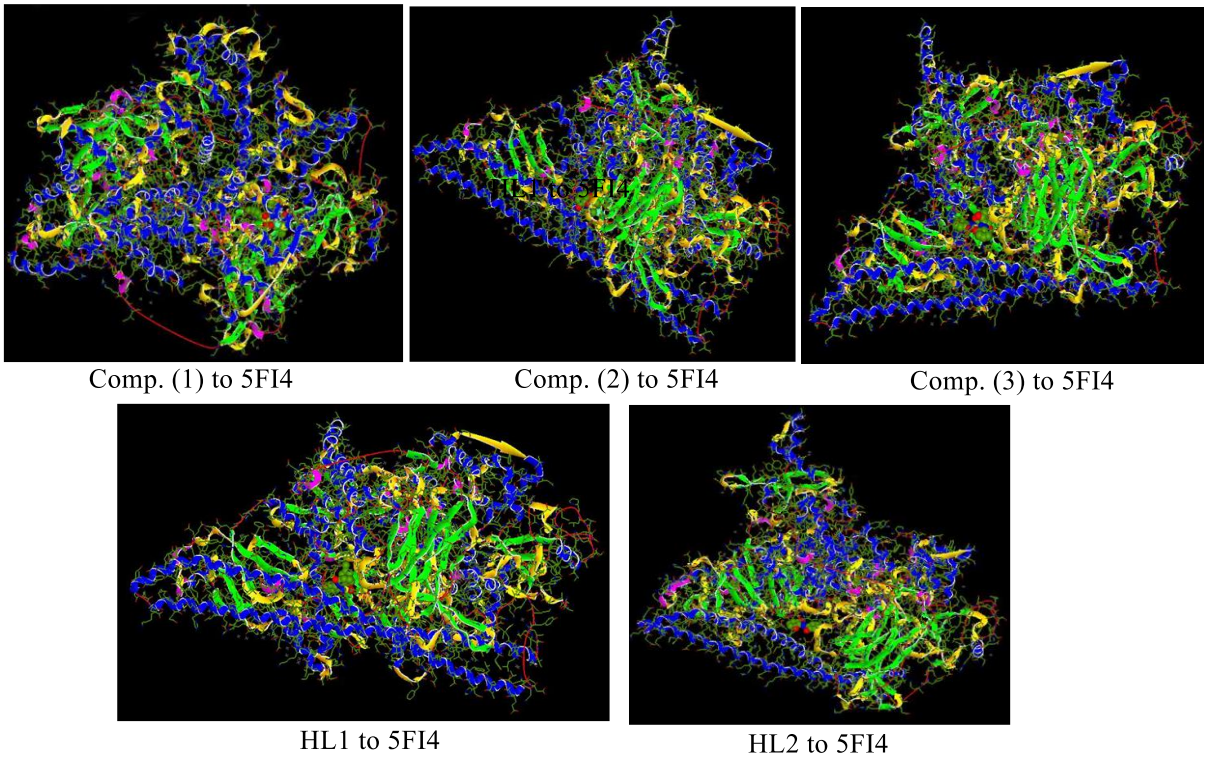

Figure 7. The binding region of the Comp. (1)-(3) and HL1, HL2 with the 5FI4 target protein.

Table 7. The binding energies (kJ/mol) of the Comp. (1)-(3) and HL1, HL2 with the target proteins.

Ligand/Target Protein	The Binding Energies (kJ/mol)
Comp. (1) to 4M5W	-387.52
Comp. (2) to 4M5W	-285.44
Comp. (3) to 4M5W	-364.88
HL1 to 4M5W	-300.02
HL2 to 4M5W	-240.80
Comp. (1) to 5FI4	-399.63
Comp. (2) to 5FI4	-297.80
Comp. (3) to 5FI4	-385.323
HL1 to 5FI4	-336.64
HL2 to 5FI4	-247.04

The interaction energies between the identified target proteins with the mentioned molecules in Table 7 were given. According to Table 7, the complexes were evaluated among themselves and the ligands among themselves. As a result of the comparison of the binding energies between the examined molecules and the target proteins, it was found to be highly compatible with the experimentally determined anti-cancer activities. The target protein thus selected is highly compatible for the molecules studied. Complex 1 has the highest inhibitory activity relative to the binding energy of complexes and ligands with the target protein, and the overall inhibition activity sequences are as follows.

Comp. (1) > Comp. (3) > Comp. (2)
HL1> HL2
} According to 4M5W

Comp. (1) > Comp. (3) > Comp. (2)
HL1> HL2
} According to 5FI4

4. CONCLUSION

In this work, experimentally synthesized HL1 and HL2 ligands and their platinum complexes were investigated using computational chemistry methods.

Benchmark analysis was carried out by considering the experimental structural parameters for the Comp.(1)-(3). The optimum level according to the correlation coefficients derived from the bond lengths and bond angles was determined as B3LYP/LANL2DZ/6-31G+(d).For ligands, the calculations were made at B3LYP/6-31G(d)+. The optimizations of the ligands and complexes were shown by giving atomic numbers. It was found that the calculated values by experimental bond stretching are compatible for ligands and complexes. The type of vibrational modes corresponding to the bond stretching modes was labeled. For the Comp. (1)-(3) with ligands HL1 and HL2, the experimental and calculated chemical shifts of ^{1}H, ^{13}C and ^{19}F-NMR were compared and atom assignment was performed. The relationship between the IC50 values obtained against cancer cells A2780 and A2780-CP70 experimentally and the quantum chemical parameters such as HOMO energy (E_{HOMO}), LUMO energy (E_{LUMO}), LUMO-HOMO energy vacancy (ΔE), hardness (η), softness (σ), electronegativity (χ) and chemical potential (μ) of mentioned ligands and complexes was examined. The quantum chemical parameters obtained for the ligands were found to be highly consistent with the biological activities. When the quantum chemical parameters of the complexes were compared with the experimental IC50 values, results were obtained which were in accordance with the LUMO energy sequence. MEP maps were examined for determined the electrophilic and nucleophilic regions of ligands and complexes. Finally, the binding energies obtained using molecular docking for proteins and investigated molecules were highly consistent with the experimental IC50 values.

REFERENCES

[1] Hu Y., Tabor R.F., Wilkinson B.L., Sweetness and light: design and applications of photo-responsive glycoconjugates, Org. Biomol. Chem., 13-8 (2015) 2216−2225.

[2] Velema W.A., Szymanski W., Feringa B.L., Photopharmacology: beyond proof of principle, J. Am. Chem. Soc., 136-6 (2014) 2178−2191.

[3] Li J., Wang X., Liang X., Modification of Nucleic Acids by Azobenzene Derivatives and Their Applications in Biotechnology and Nanotechnology, Chem. Asian J., 9-12 (2014) 3344−3358.

[4] Kundu P.K., Klajn R., Watching single molecules move in response to light, ACS Nano, 8-12 (2014) 11913−11916.

[5] García-Iriepa C., Marazzi M., Frutos L.M., Sampedro D., E/Z Photochemical switches: syntheses, properties and applications, RSC Adv., 3-18 (2013) 6241−6266.

[6] Wegner H.A., Azobenzenes in a new light—Switching in vivo, Angew. Chem., Int. Ed., 51-20 (2012) 4787−4788.

[7] Bandara H.M.D., Burdette S.C., Photoisomerization in different classes of azobenzene, Chem. Soc. Rev., 41-5 (2012) 1809−1825.

[8] Merino E., Synthesis of azobenzenes: the coloured pieces of molecular materials, Chem. Soc. Rev., 40-7 (2011) 3835−3853.

[9] Beharry A.A., Woolley G.A., Azobenzene photoswitches for biomolecules, Chem. Soc. Rev., 40-8 (2011) 4422− 4437.

[10] Hamon F., Djedaini-Pilard F., Barbot F., Len C., Azobenzenes—synthesis and carbohydrate applications, Tetrahedron, 65-49 (2009) 10105−10123.

[11] Samanta S., Ghosh P., Goswami S., Recent advances on the chemistry of transition metal complexes of 2-(arylazo) pyridines and its arylamino derivatives, Dalton Trans., 41-8 (2012) 2213−2226.

[12] Muggia F.M., Recent updates in the clinical use of platinum compounds for the treatment of gynecologic cancers., In Semin. Oncol., WB Saunders, 31 (2004) 17–24.

[13] Belani C.P., Recent updates in the clinical use of platinum compounds for the treatment of lung, breast, and genitourinary tumors and myeloma, In Semin.Oncol., WB Saunders, 31 (2004) 25–33.

[14] Cleare M.J., Hoeschele J.D., Antilt umour Platinum Compounds, Platin. Met. Rev., 17 (1973) 2–13.

[15] Cleare M.J., Hoeschele J.D., Studies on the antitumor activity of group VIII transition metal complexes, Bioinorg. Chem., 2-3 (1973) 187–210.

[16] Endresi, H., 1985. A hydrogen-bridged dimeric stacked structure in a dioximato complex: (oxamide oximato)(oxamide oxime) platinum (II) iodide dihydrate, $[Pt(C_2H_5N_4O_2)(C_2H_5N_4O_2)]I.2H_2O$. Acta Cryst. C41, 1047-1049.

[17] Guedes da Silva, M. F. C., Izotova, Y. A., Pombeiro, A. J. L., Kukushkin, V. Y., 1998. Manifestation of redox duality of 2-propanone oxime: Pt(II)-assisted reduction versus Pt (IV) - mediated oxidation of Me2O= NOH species. Inorg. Chim. Acta. 277, 83-88.

[18] Makarycheva-Mikhailova, A. V., Haukka, M., Bokach, N. A., Garnovskii, D. A., Galanski, M., Keppler, B. K., Pomberio, A. J. L., Kukushkin, V. Y., 2002. Platinum(IV)-mediated coupling of dione monoximes and nitriles: a novel reactivity pattern of the classic oxime-based chelating ligands. New J. Chem. 26, 1085-1091.

[19] Köcher, S., Lutz, M., Spek, A. L., Walfort, B., Rüffer, T., van Klink, G. P. M., van Koten, G., Lang, H., 2008. Oxime-substituted NCN-pincer palladium and platinum halide polymers through non-covalent hydrogen bonding $(NCN=[C_6H_2(CH_2NMe_2)2\text{-}2,6]-)$. Journal of Organometallic Chemistry. 693, 2244-2250.

[20] Grabmann, G., Meier, S. M., Scaffidi-Domianello, Y. Y., Galanski, M., Keppler, B. K., Hartinger, C. G., 2012. Capillary zone electrophoresis and capillary zone

electrophoresis– electrospray ionization mass spectrometry studies on the behavior of anticancer cis- and trans- [dihalidobis(2-propanone oxime)platinum(II)] complexes in aqueous solutions. Journal of Chromatography A. 1267, 156-161.

[21] Deo C., Bogliotti N., Métivier R., Retailleau P., Xie J., Photoswitchable arene ruthenium complexes containing o-sulfonamide azobenzene ligands, Organometallics, 34-24 (2015) 5775−5784.

[22] Samper K.G., Marker S.C., Bayón P., MacMillan S.N., Keresztes I., Palacios Ò., Wilson J.J., Anticancer activity of hydroxy- and sulfonamide-azobenzene platinum (II) complexes in cisplatin-resistant ovarian cancer cells, Journal of Inorganic Biochemistry, 174 (2017) 102–110.

[23] Dennington II R. D.; Keith T.A.; Millam J.M. GaussView 5.0, Wallingford, CT, 2009.

[24] Frisch M J, Trucks G W, Schlegel H B, Scuseria G E, Robb M A, Cheeseman J R, Scalmani G, Barone V, Mennucci B & Petersson G A, et al. Gaussian, Inc., Wallingford CT, 2010.

[25] Zhurko G.A., Zhurko D.A., ChemCraft, version 1.6, 2009. (*http://www.chemcraftprog.com*)

[26] Roothaan C. C. J., New developments in molecular orbital theory, Rev. Mod. Phys., 23-2 (1951) 69.

[27] Awad M.K., Mustafa M.R., Computational simulation of the molecular structure of some triazoles as inhibitors for the corrosion of metal surface, Journal of Molecular Structure: THEOCHEM., 959 (2010) 66–74.

[28] Becke A.D., Density-functional thermochemistry. III. The role of exact Exchange, The Journal of Chemical Physics, 98-7 (1993) 5648–5652.

[29] Tüzün B., Kaya C., Investigation of DNA–RNA Molecules for the Efficiency and Activity of Corrosion Inhibition by DFT and Molecular Docking, Journal of Bio- and Tribo-Corrosion 4-69 (2018) 2-11.

[30] Üngördü A., Tezer N., Effect on frontier molecular orbitals of substituents in 5-position of uracil base pairs in vacuum and water, Journal of Theoretical and Computational Chemistry, 16-07 (2017) 1750066.

[31] Sayin, K., Üngördü, A., Investigation of anticancer properties of caffeinated complexes via computational chemistry methods, Spectrochimica Acta Part A: Molecular and Biomolecular Spectroscopy, 193 (2018) 147-155.

[32] Sarigul M., Erkan S.K., Deveci P., Atabey H., KarakasbD., Kurtoglu M., Multi-properties of a new azo-Schiff base and its binuclear copper (II) chelate: Preparation, spectral characterization, electrochemical, potentiometric and modeling studies. Journal of Molecular Structure, 1149 (2017) 520-529.

[33] Karakaş D., Erkan S.K., Theoretical investigation on the vibrational and electronic spectra of three isomeric forms of dicobalt octacarbonyl, Journal of Molecular Structure, 1062 (2014) 77-81.

[34] Erkan S.K, Sayın K., Karakaş D., Theoretical Studies on Eight Oxovanadium (IV) Complexes with Salicylaldehyde and Aniline Ligands, Hacettepe J Biol Chem, 42 (2014) 337-342.

[35] Dracǐnsky M., Bour P., Hodgkinson P., Temperature dependence of NMR parameters calculated from path integral molecular dynamics simulations, J. Chem. Theory Comput., 12-3 (2016) 968−973.

[36] Pearson R. G., Absolute electronegativity and hardness: application to inorganic chemistry, Inorg. Chem., 27-4 (1988) 734-740.

[37] Koopmans T., Über die Zuordnung von Wellenfunktionen und Eigenwerten zu den einzelnen Elektronen eines Atoms, Physica, 1 (1934) 104.

[38] Muscia G.C., Cazorla S.I., Frank F.M., Borosky G.L., Buldain G.Y., Asís S.E., Malchiodi E.L., Synthesis, trypanocidal activity and molecular modeling studies of 2-alkylaminomethylquinoline derivatives, Eur. J. Med. Chem., 46-9 (2011) 3696-3703.

[39] Kushwaha P.S., Mishra P.C., Relationship of hydrogen bonding energy with electrostatic and polarization energies and molecular electrostatic potentials for amino acids: an evaluation of the lock and key model, Int. J. Quant. Chem., 76-6 (2000) 700-713.

[40] Wagener M., Sadowysky J., Gasteiger J., Autocorrelation of molecular surface properties for modeling corticosteroid binding globulin and cytosolic Ah receptor activity by neural networks, J. Am. Chem. Soc., 117-29 (1995) 7769– 7775.

[41] Sayin K., Karakaş D., Erkan S.K., Alagöz Sayin T., Computational study of some fluoroquinolones: Structural, spectral and docking investigations, Journal of Molecular Structure, 1156 (2018) 172-181

[42] Qin D., Wang W., Lei H., Luo H., Cai H., Tang C., Wang T., CDDO-Me reveals USP7 as a novel target in ovarian cancer cells, Oncotarget, 7-47 (2016) 77096.

[43] Han W., Menezes D.L., Xu Y., Knapp M.S., Elling R., Burger M.T., Ni Z.J., Smith A., Lan J., Williams T.E., Verhagen J., Huh K., Merritt H., Chan J., Kaufman S., Voliva C.F., Pecchi S., Discovery of imidazo [1, 2-a]-pyridine inhibitors of pan-PI3 kinases that are efficacious in a mouse xenograft model. Bioorganic & medicinal chemistry letters, 26-3 (2016) 742-746.